Supplemental information

Rationally designed immunogens

enable immune focusing

following SARS-CoV-2 spike imprinting

Blake M. Hauser, Maya Sangesland, Kerri J. St. Denis, Evan C. Lam, James Brett Case, Ian W. Windsor, Jared Feldman, Timothy M. Caradonna, Ty Kannegieter, Michael S. Diamond, Alejandro B. Balazs, Daniel Lingwood, and Aaron G. Schmidt
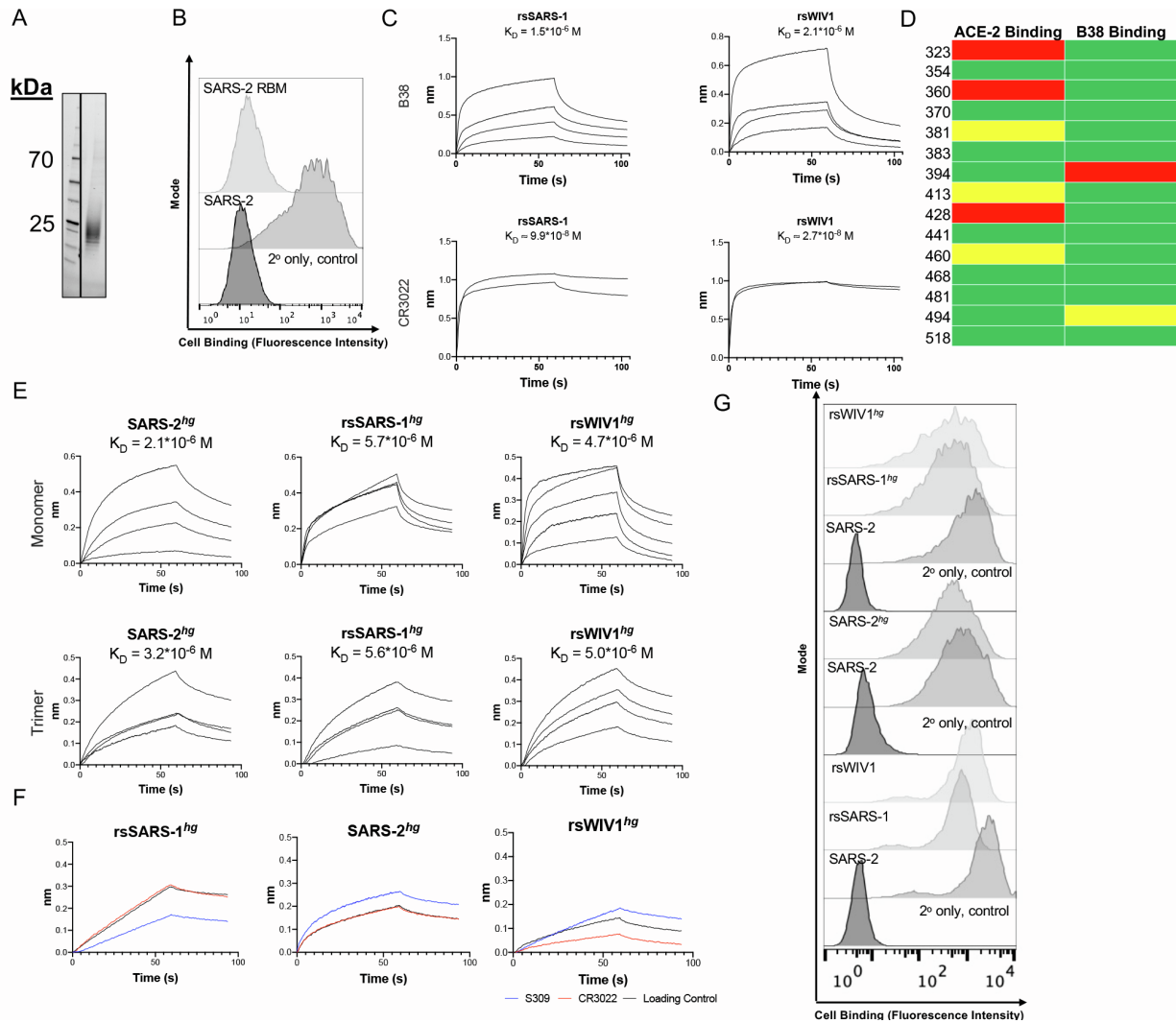
Figure S1 (related to **Fig. 1**). **Biochemical validation of resurfaced and hyperglycosylated immunogens. (A)** SDS-Page gel analysis of the SARS-2 receptor binding motif (RBM) construct with HRV 3C-cleavable 8xHis and streptavidin binding peptide (SBP) tags. Gel lanes containing unrelated samples have been removed. **(B)** ACE2 cell binding assay results for the SARS-2 RBM construct at 1 μM. **(C)** After grafting the SARS-2 RBM onto the SARS-1 and WIV1 RBDs, conformationally specific Fabs B38 and CR3022 were used to confirm that these epitopes remained intact with comparable affinity to wild-type (9.7*10^{-7} M for B38 Fab and SARS-2 RBD; 2.7*10^{-8} M for CR3022 Fab and SARS-1 RBD; 3.7*10^{-8} M for CR3022 Fab and WIV1 RBD). FAB2G sensors were used with immobilized fabs. rsSARS-1 and rsWIV1 were the analytes. Titrations with B38 Fab were performed at 10 μM, 5 μM, 1 μM, and 0.5 μM. Titrations with CR3022 Fab were performed at 10 μM and 5 μM. Vendor-supplied software was used to generate an apparent K_D, or an approximate K_D in the case of titrations with two runs. **(D)** Candidate glycans were tested individually in the context of the SARS-CoV-2 RBD. All glycans were designed to mask epitopes outside the RBM. Therefore, biochemical validation was performed by assessing binding to the RBM-directed conformationally specific antibody B38 via single-hit BLI using FAB2G sensors with the RBD of interest as the analyte at 10 μM. Binding to ACE2 was also

assessed via an ACE2 cell binding assay with antigen concentrations at 1 µM. Binding was binned subjectively into three categories: minimal (red), substantially reduced (yellow), and roughly intact (green). **(E)** Conformationally specific Fab B38 was used to assess continued accessibility of the SARS-2 RBM in both monomeric and trimeric hyperglycosylated constructs. FAB2G sensors were used with immobilized fabs; hyperglycosylated coronavirus proteins were the analytes. Titrations with B38 Fab were performed at 7.5 µM, 5 µM, 2.5 µM, and 1 µM (rsSARS-1^{hg} trimer, rsWIV1^{hg} trimer); 5 µM, 2.5 µM, 1 µM, and 0.5 µM (SARS-2^{hg} trimer, SARS-2^{hg} monomer); 10 µM, 7.5 µM, 5 µM, 3.75 µM, and 2.5 µM (rsWIV1^{hg} monomer); 10 µM, 7.5 µM, 5 µM, and 2.5 µM (rsSARS-1^{hg} monomer). Vendor-supplied software was used to generate an apparent K_D. **(F)** BLI with conformationally specific Fabs CR3022 and S309 at 10 µM was compared to loading controls for each of the hyperglycosylated monomers. The similarity in these traces to the no-antibody loading control confirms a lack of binding. **(G)** ACE2 cell binding assay results for resurfaced and hyperglycosylated constructs at 1 µM.
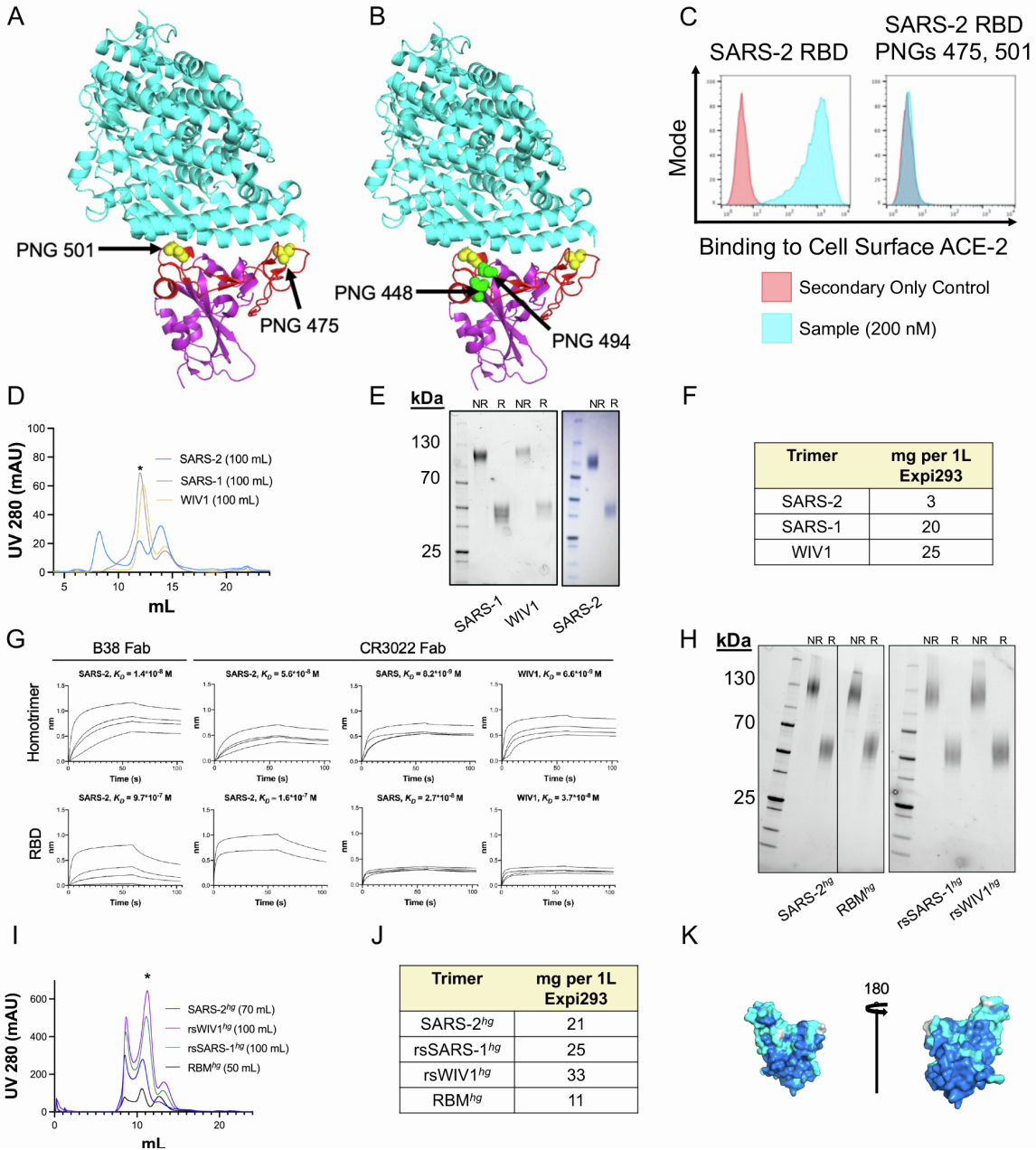
Figure S2 (related to **Fig. 1**). **Immunogen production and biochemical validation. (A, B)** Design and expression of two different versions of the SARS-2 RBD with additional putative N-linked glycosylation sites (PNGs) engineered onto the RBM. One construct has glycosylation sites at positions 475 and 501, while the other construct has glycosylation sites at positions 475, 501, 448, and 494. The latter is the RBM^{hg} construct. ACE2 is shown in cyan, the RBM is shown in red, and the non-RBM portion of the SARS-2 RBD is shown in purple. (PDB: 6M0J) (**C**) The presence of glycans at positions 475 and 501 alone is sufficient to abrogate ACE2 binding to the RBM. (**D**) Representative size exclusion trace with (*) marking the trimeric constructs. Fractions in this peak were pooled and used for immunizations. Quantity of Expi293 transfection is in parentheses next to each label. (**E**) SDS-PAGE analysis of purified trimers following removal of the affinity purification tags under non-reducing (NR) and reducing (R) conditions. The engineered disulfide bond at the C-terminus of the hyperglycosylated GCN4 tag separated under reducing

conditions. Panel includes monomeric RBDs run under reducing conditions for comparison. Gel lanes containing unrelated samples have been removed. **(F)** Protein yields for purified trimeric constructs in Expi293 cells. **(G)** Conformationally specific Fabs CR3022 and/or B38 were used to verify that trimer affinity was comparable (or greater than, due to increased avidity) wild-type RBD affinity. Fabs were immobilized to FAB2G sensors, and coronavirus proteins were the analytes. Trimers were titrated at 1 µM, 750 nM, 500 nM, and 250 nM. Monomeric SARS-1 and WIV1 RBDs were titrated at 10 µM, 5 µM, 2.5 µM, and 1 µM. Monomeric SARS-2 RBD was titrated at 10 µM, 1 µM, 500 nM, and 100 nM with B38 Fab and at 10 µM, 5 µM, 750 nM, and 250 nM with CR3022 Fab. Apparent K_D was obtained by vendor-supplied software. **(H)** SDS-Page gel analysis of purified and cleaved trimeric constructs under non-reducing (NR) and reducing (R) conditions, showing the dissociation of the disulfide bond in the hyperglycosylated GCN4 tag (hgGCN4^{cys}) under reducing conditions. Gel lanes containing unrelated samples have been removed. **(I)** Representative size exclusion chromatography traces for trimeric constructs. The trimer peak is marked with "*", and fractions from this peak were pooled for HRV 3C cleavage and use as immunogens. Quantity of Expi293 transfection is in parentheses next to each label. **(J)** Protein yields for purified trimeric hyperglycosylated constructs in Expi293 cells. **(K)** Strict amino acid conservation across the SARS-2 RBD (Genbank MN975262.1), SARS-1 RBD (Genbank ABD72970.1), and WIV1 RBD (Genbank AGZ48828.1) is depicted using dark blue on the structure for matches between all three genes, light blue for matches between two genes, and silver for positions where all genes differ (PDB: 6M0J).

Figure S3 (related to **Fig. 2**). **Serum antigenicity assessed via ELISA.** Serum following immunizations from the Trimer **(A)**, Trimer^{hg} **(B)**, Cocktail^{hg} **(C)**, RBM^{hg} **(D)**, and Trivalent **(E)** cohorts was assayed in ELISA at day 35 with different coronavirus antigens. Bars represent mean ± SEM. The SARS-2 spike refers to the double-proline stabilized spike used in the prime immunization, while all of the other coating antigens are RBDs. Statistical significance was determined using Kruskal-Wallis test with post-hoc analysis using Dunn's test corrected for multiple comparisons, and pairwise comparisons without pictured bars were not significant (* = p < 0.05, ** = p < 0.01, *** = p < 0.001, **** = p < 0.0001). Selected titers from **Fig. S3A-E** are shown in **Fig. 2A**; differences in levels of statistical significance are due to the fact that multiple comparisons were performed in **Fig. S3A-E**. **(F)** A serum ELISA was performed for Trivalent cohort with an irrelevant protein (influenza hemagglutinin head) tagged with the hyperglycosylated GCN4 tag (HA-GCN4) to measure tag-directed antibody responses. The Trivalent cohort was selected because it had the highest serum ELISA titers. For the coating HA-

GCN4 protein, a purification size exclusion trace (fractions in the peak marked with "*" were pooled) and an SDS-PAGE gel run under non-reducing (NR) and reducing (R) conditions are shown. Gel lanes containing unrelated samples have been removed. **(G)** Serum ELISAs were performed against the relevant hyperglycosylated immunogens for the Trimer^{hg} and Cocktail^{hg} cohorts. There was no statistically significant difference in endpoint titers within the Trimer^{hg} or Cocktail^{hg} cohorts across these coating antigens, as determined by the Mann-Whitney U test and the Kruskal-Wallis test, respectively. Bars represent mean ± SEM. **(H)** For all cohorts, day 35 serum samples were used in ELISAs to assess binding to RaTG13 and SHC014 RBDs. Bars represent mean ± SEM. No statistical comparisons were performed.

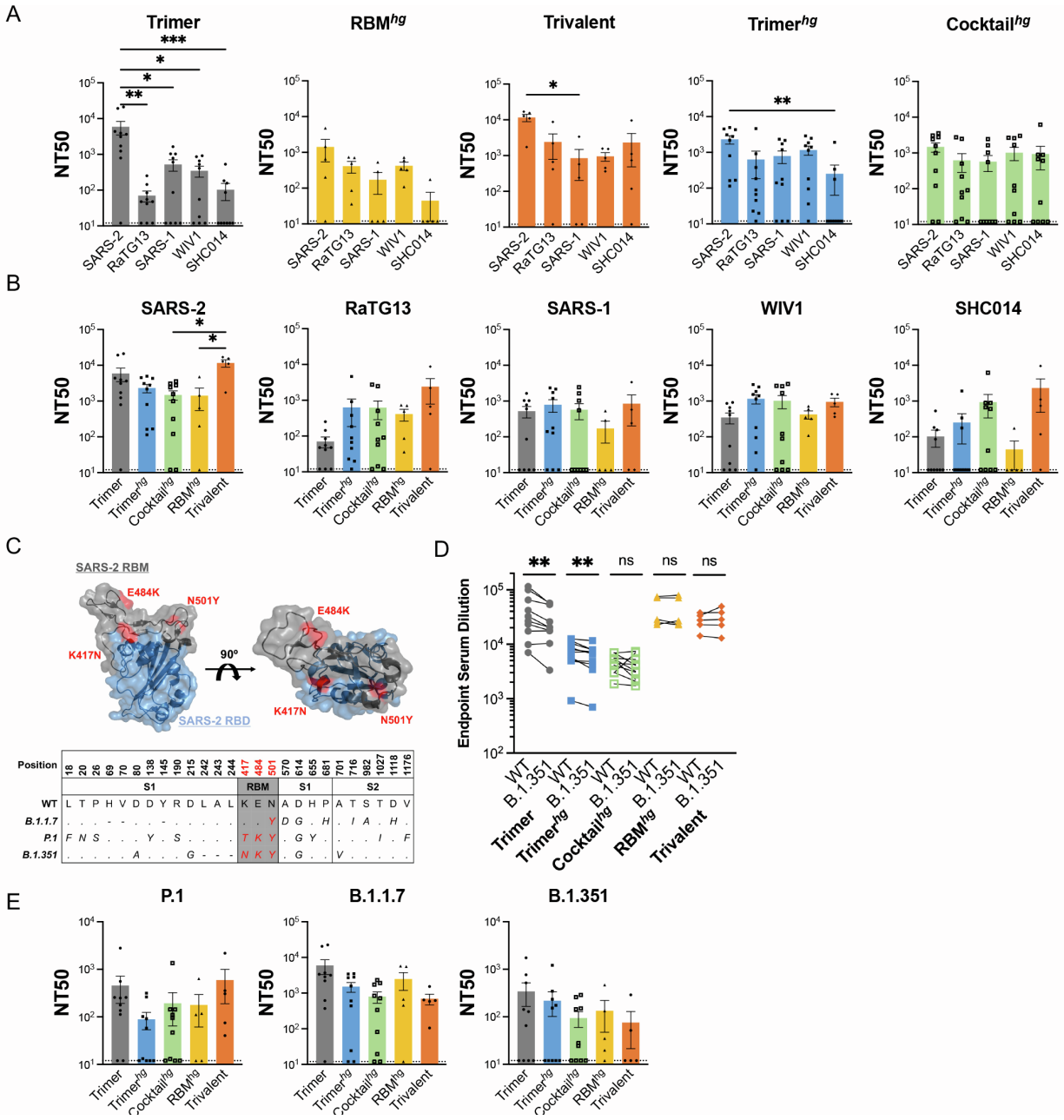**Figure S4** (related to **Fig. 3**). **Neutralization against related sarbecoviruses and SARS-2 variants of concern. (A)** Day 35 serum from all mice was assayed for neutralization against SARS-2, RaTG13, SARS-1, WIV1, and SHC014 pseudoviruses. Statistical significance was determined using the Kruskal-Wallis test with post-hoc analysis using Dunn's test corrected for multiple comparisons, and pairwise comparisons without pictured bars were not significant (* = p < 0.05, ** = p < 0.01, *** = p < 0.001). Bars represent mean ± SEM. **(B)** Pseudovirus neutralization assays were used to calculate NT50 values for SARS-2, SARS-1, WIV1, RaTG13, and SHC014 from all cohorts. All NT50s are from day 35 sera. Statistical significance was determined using the Kruskal-Wallis test with post-hoc analysis using Dunn's test corrected for multiple

comparisons in the case of a significant Kruskal-Wallis test, and pairwise comparisons without pictured bars were not significant (* = p < 0.05). Bars represent mean ± SEM. **(C)** Structural depiction of SARS-2 variant RBD mutations for B.1.351 (red), as well as ACE2 contact residues (cyan). (PDB: 6M0J) Sequences depict all spike mutations across select variants. **(D)** Day 35 serum was assayed in ELISA against SARS-2 RBD (WT) and SARS-2 RBD with K417N, E484K, and N501Y mutations (B.1.351). Statistical significance was determined using the Wilcoxon sign rank test (* = p < 0.05, ** = p < 0.01; ns = not significant). **(E)** Pseudovirus neutralization assays were used to calculate NT50 values for P.1, B.1.1.7, and B.1.351 from all cohorts. All NT50s are from day 35 sera. Statistical significance was determined using the Kruskal-Wallis test; no pairwise differences are statistically significant. Bars represent mean ± SEM.
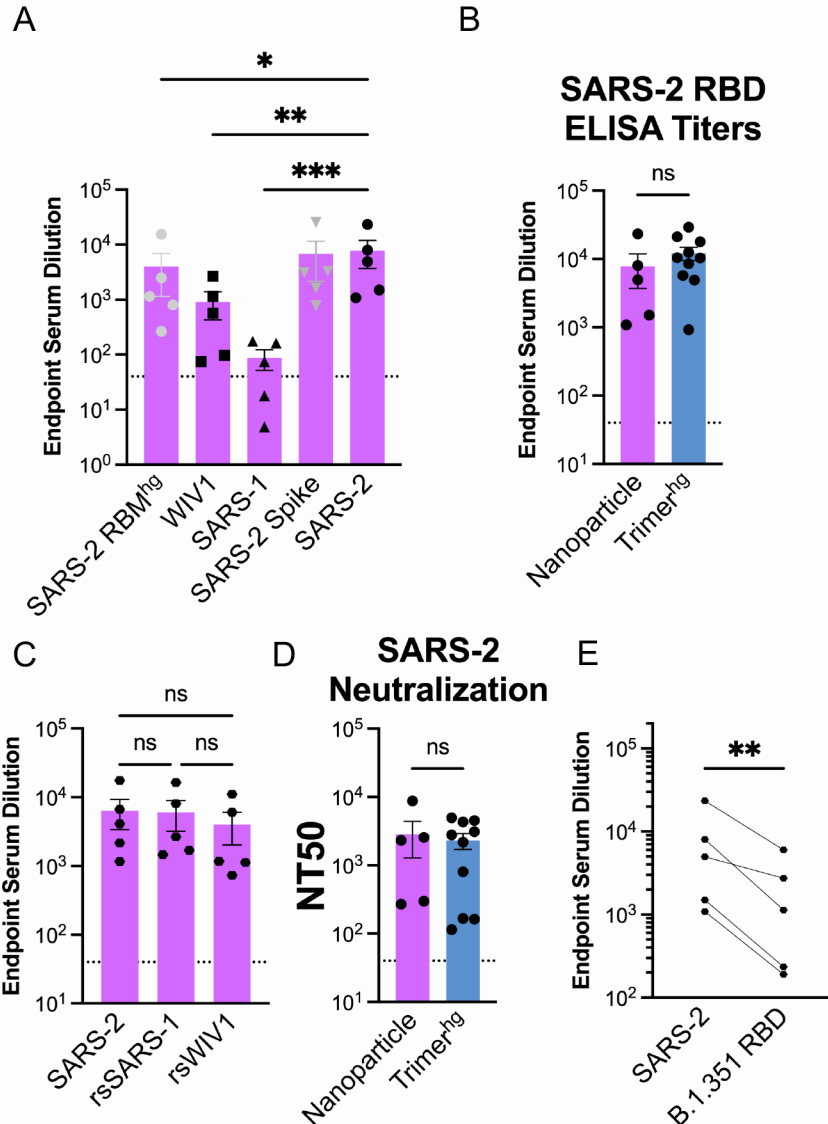
Figure S5 (related to **Fig. 4**). **Serum antigenicity for the Nanoparticle cohort**. **(A)** Serum following immunization was assayed in ELISA at day 35 with different coronavirus antigens. Statistical significance was determined using the Kruskal-Wallis test with post-hoc analysis using Dunn's test corrected for multiple comparisons, and pairwise comparisons without pictured bars were not significant (* = $p < 0.05$, ** = $p < 0.01$, *** = $p < 0.001$). Bars represent mean ± SEM. **(B)** Comparison of day 35 SARS-2 RBD ELISA endpoint titers in the Nanoparticle and Trimer[hg] cohorts. Statistical significance was determined using the Mann-Whitney U test (ns = not significant). Bars represent mean ± SEM. **(C)** Day 35 serum samples assayed against rsSARS-1 and rsWIV1 RBDs no longer show statistically significant differences in binding compared to SARS-2 RBD as determined using the Kruskal-Wallis test with post-hoc analysis using Dunn's test corrected for multiple comparisons. Bars represent mean ± SEM. **(D)** Comparison of day 35 SARS-2 pseudovirus neutralization in the Nanoparticle and Trimer[hg] cohorts. Statistical significance was determined using the Mann-Whitney U test (ns = not significant). Bars represent

mean ± SEM. **(E)** Day 35 serum was assayed in ELISA against SARS-2 RBD (WT) and SARS-2 RBD with K417N, E484K, and N501Y mutations (B.1.351). Statistical significance was determined using the Wilcoxon sign rank test (* = $p < 0.05$, ** = $p < 0.01$).
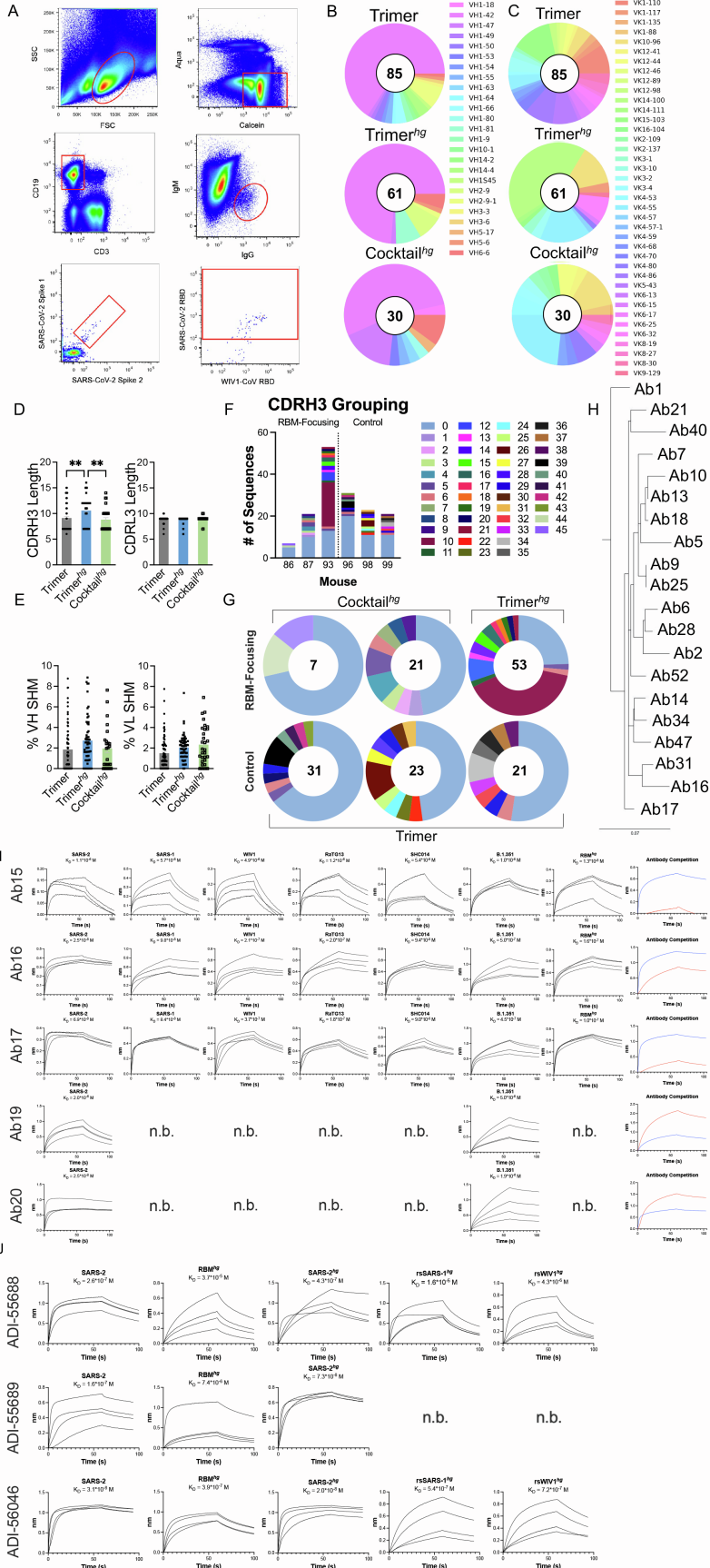
Figure S6 (related to **Fig. 5**). **SARS-2 RBD-directed B cell characteristics. (A)** Gating scheme for isolating IgG+ B cells that are SARS-2 spike double-positive and SARS-CoV-2 RBD positive. Spleens were harvested at day 42 and SARS-2 RBD-directed IgG+ B cells were isolated via flow cytometry and sequenced. B cell receptor sequencing was used to characterize **(B)** heavy and **(C)** light chain V-gene usage. All gene families listed are *01 except VH1-84*02. Complementarity determining region 3 (CDR3) length **(D)** and percent somatic hypermutation (SHM) **(E)** were also analyzed for each sequence. SHM was not analyzed for cohorts with uncertain IMGT V-gene assignments. Statistical significance was determined using the Kruskal-Wallis test with post-hoc analysis using Dunn's test corrected for multiple comparisons, and pairwise comparisons without pictured bars were not significant (* = $p < 0.05$, ** = $p < 0.01$). Bars represent mean ± SEM. Within each mouse, clonal lineages were analyzed on the basis of CDRH3 similarity. CDRH3 groupings are represented by count **(F)** and proportion **(G)** within each mouse. Not all sequences were successfully grouped into lineages. **(H)** Phylogenetic tree of a large clonal lineage containing Ab16 and Ab17 generated using Cloanalyst to infer common ancestors. **(I)** BLI was performed using Fabs representative of lineages expanded in RBM-focusing cohorts. Ni-NTA biosensors were used with Fabs bound to the sensor using the 8xHis tag and RBDs in solution as the analyte. Titrations were performed at 10 µM, 5 µM, 2.5 µM, and 1 µM. Vendor-supplied software was used to generate an apparent K_D. **(J)** Conformationally specific Fabs ADI-55688, ADI-55689, and ADI-56046, which target a conserved RBM epitope, were used to assess binding to the RBM^{hg}, SARS-2^{hg}, rsSARS-1^{hg}, and rsWIV1^{hg} monomers via BLI. FAB2G sensors were used with immobilized fabs; coronavirus proteins were the analytes. Titrations were performed at 10 µM, 5 µM, 2.5 µM, and 1.25 µM (SARS-2 RBD and SARS-2^{hg} with ADI-55689, SARS-2 RBD and SARS-2^{hg} with ADI-56046, all titrations with RBM^{hg}); 3 µM, 1.5 µM, 0.75 µM, and 0.375 µM (rsSARS-1^{hg} and rsWIV1^{hg} with ADI-56046); 10 µM, 5 µM, 2.5 µM, and 1 µM (all titrations with ADI-55688 except RBM^{hg}). Minimal binding was detected to ADI-55689 Fab with rsSARS-1^{hg} and rsWIV1^{hg}. Vendor-supplied software was used to generate an apparent K_D.
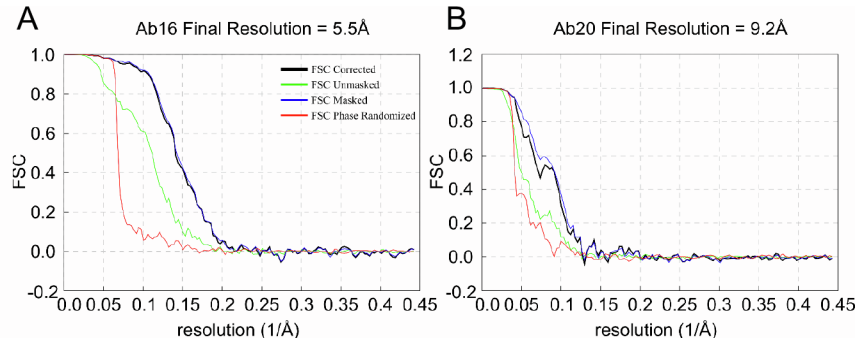
Figure S7 (related to **Fig. 6**). **Supporting data for moderate-resolution structures of Ab16 and Ab20 complexes**. Fourier shell correlation plots show the nominal resolution of the spike complex of Ab16 is 5.5 Å (**A**) and Ab20 is 9.2 Å (**B**) (0.143 cutoff).

Antibody	VH Sequence	VL Sequence
Ab15	GAGGTCCAGCTGCAGCAGTCTGGACCTGAGCTGGTGAAGCCTGGGGCTTCAGT GAAGATATCCTGCAGCAGTCTTGGTTACTCACTGGCTACTACATGAACTGG GTGAAGCAAAGTCCTGAAAAGAGCCTTGAGTGGATTGGAGAGATTAATCCTAACTT TGGTGGTACTACCTACAACCAGAAGTTCAAGGCCAAGGCCACATTGACTGTAGAC AAATCCTCCAGCACAGCCTACATGCAGCTCAAGAGCCTGACATCTGAGGACTCTG CAGTCTATTACTGTGCAAGATACTATGGTAACCTCTATGCTATGGACTACTGGGGT CAAGGAACCTCAGTCACCGTCTCC	GACATCCTGATGACCCAGTCTCCATCCTCCATGTCTGTATCTCTGGGAGACACAG TCAGCATCACTTGCCATGCAAGTCAGGGCATTAGCAGTAATATAGGGTGGTTGCA GCAGAAACCAGGGAAATCATTTAAGGGCCTGATCTATCATGGAACCAACTTGGAA GATGGAGTTCCATCAAGGTTCAGTGGCAGTGGATCTGGAGCAGCTTATTCTCTCA CCATCAGCAGCCTGGAATCTGAAGATTTTGCAGACTATTACTGTGTACAGTATACT CATTTTCCGTACACGTTCGGAGGGGGGGACCAAGCTGGAAATAAAA
Ab16	GAGGTCCAGCTGCAGCAGTCTGGACCTGAGCTGGTGAAGCCTGGGGCTTCAGT GAAGATATCCTGCAAGGCTTCTGGTTACTCATTTAATAACTACTACATGAACTGG TGAAGCAGAGTCCTGAAAAGAGCCTTGAGTGGATTGGAGAGATTAATCCTAACTC TGGTTATACTTCCTACAACCAGAAGTTCAGGGCCAAGGCCACATTGACTGTAGACA AATCCTCCACCACAGCCTACATGCAGCTCAAGAGCCTGACATCTGAGGACTCTGC GGTCTATTACTGTGCAAGATACTTTGGTAACCTCTTTGCTATGGACTTCTGGGGT CAAGGAACCTCAGTCACCGTCTCC	GACATCCTGATGACCCAATCTCCATCCTCCATGTCTGTATCTCTGGGAGACACAGT CAGCATCACTTGCCATGCAAGTCAGGGCATTGGCAGTAATATAGGGTGGTTGCAG CAGAAACCAGGGAAATCATTTAAGGGCCTGATCTATCATGGAACCAACTTGGAAGA TGGAGTTCCATCAAGGTTCAGTGGCAGTGGATCTGGAGCAGATTATTCTCTCACC ATCAGCAGCCTGGAATCTGAAGATTTTGCAGACTATTACTGTGTACAGTATGTTCA GTTTCCGTACACGTTCGGAGGGGGGGACCAAGCTGGAAATAAAA
Ab17	GAGGTCCAGCTGCAGCAGTCTGGACCTGAGCTGGTGAAGCCTGGGGCTTCAGT GAAGATATCCTGCAAGGCTTCTGGTTACTCATTCACTGACTACTACATGAACTGGG TGAAGCAAAGTCCTGAAAAGAGCCTTGAGTGGATTGGAGAGATTAATCCTAACTC GGTGGTACTACCTACAACCAGAAGTTCAAGGCCAAGGCCACATTGACTGTAGACA AATCCTCCAGCACAGCCTACATGCAGCTCAAGAGCCTGACATCTGAGGACTCTGC AGTCTATTACTGTGCAAGATACTATGGTAACCTCTATGCTATGGACTACTGGGGTC AAGGAACCTCAGTCACCGTCTCCTCA	GACATCCTGATGACCCAATCTCCATCCTCCATGTCTGTATCTCTGGGAGACACAGT CAGCATCACATGCCATGCAAGTCAGGGCATAAGTAGTAATATAGGGTGGTTGCAG CAGAAACCAGGGAAATCATTTAAGGGCCTGATCTATCATGGAACCAACTTGGAAGA TGGAGTTCCATCAAGGTTCAGTGGCAGTGGATCTGGAGCAGATTATTCTCTCACC ATCAGCAGCCTGGAATCTGAAGATTTTGCAGACTATTACTGTGTACAGTATGTTCA GTTTCCGTACACGCTCGGAGGGGGGGACCAAGCTGGAAATAAAA
Ab19	CAGGTTCAGCTGCAGCAGTCTGGAGCTGAGCTGGCGAGGCCTGGGGCTTCAGT GAAGCTGTCCTGCAAGGCTTCTGGCTACCCCTTCACAAGCTATGGTATAAACTGG GTGAAGCAGAGAACTGGACAGGGCCTTGAGTGGATTGGAGAGATTTATCCTAGAA TTGGAAATACTTACTATAATGAGAAGTTCAAGGGCAAGGCCACACTGACTGCAGAC AAATCCTCCAGCACAGCGTACATGGAGTTCCGCAGCCTGACATCTGAGGACTCTG CGGTCTATTTCTGTGCAAGATCGTGGAATAGTAACTACGGGGAGTACTACTTTGA CTACTGGGGCCAAGGCACCACTCTCACAGTCTCC	GACATTGTGATGACCCAGTCTCACAAATTCATGTCCACATCAATAGGAGACAGGGT CAGCATCACCTGCAAGGCCAGTCACGATGTGAGTACTGCTGTAGCCTGGTATCAA CAAAAACCAGGGCAATCTCCTAAGTTACTGATTTACTGGGCATCCACCCGGCACAC TGGAGTCCCTGATCGCTTCACAGGCAGTGGATCTGGGACAGATTATACTCTCACC ATTAGAAGTGTGCAGGCAGAAGACCTGGCACTTTATTACTGTCAGCAACATTATAG CACTCCGTACACGTTCGGAGGGGGGGACCAAGCTGGAAATAAAA
Ab20	GAGGTCCAGCTGCAGCAGTCTGGACCTGAGCTGGTGAAGCCTGGGGCTTCAGT GAAGATATCCTGCAAGGCTTCTGGTTTCTCATTCACTGGCTACTCCATGAACTGGA TGAAACAAAGTCCTGAAAAGAGCCTTGAGTGGATTGGAGAAATTAATCCTACCACT GGTGGTACTACCTACAACCAGAAGTTCAAGGCCAAGGCCACATTGACTGTAGACA AATCCTCCAGCACAGCCTACATACAACTCAAGAGCCTGACATCTGAGGACTCTGCA GTCTATTACTGTGCAAGGGGCCGGGCCGACTACTGGGGCCAAGGCACCACTCTC ACAGTCTCCTCA	GACATTGTGCTCACCCAATCTCCAGCTTCTTTGGCTGTGTCTCTAGGGCAGAGAG CCACCATCTCCTGCAGAGCCAGTGAAAGTGTTGAATATTATGGCACAGGTTTAGT GCAGTGGTTCCAACAGAAACCAGGACAGCCACCCAAACTCCTCATCTATGCTGCC TCCAACGTGGAATCTGGGGTCCCTGCCAGGTTTAGTGGCAGTGGGTCTGGGACA GACTTCAGCCTCAACATCCATTCTGTGGAGGAGGATGATATTGCAATGTATTTCTG TCACCAAAGTAGGAAGCTTCCGTGGACGTTCGGTGGAGGCACCAAGCTGGAAAT CAAA

Table S1 (related to **Fig. 5**). VH and VL sequences for antibodies selected for recombinant expression and characterization as shown in **Fig. 5E**.

	Ab17 in complex with SARS-2 RBD
Wavelength (Å)	0.9792
Resolution range (Å)	74.66 - 3.5 (3.625 - 3.5)
Space group	P 41 21 2
Unit cell (Å)	207.931 207.931 86.662
(°)	90 90 90
Total reflections	513207 (54030)
Unique reflections	24538 (2401)
Multiplicity	20.9 (22.5)
Completeness (%)	99.98 (100.00)
Mean I/sigma(I)	13.89 (3.37)
Wilson B-factor	104.62
R_{merge}	0.3361 (1.898)
R_{meas}	0.3446 (1.942)
R_{pim}	0.07551 (0.4066)
CC1/2	0.998 (0.85)
CC*	0.999 (0.959)
Reflections used in refinement	24537 (2401)
Reflections used for R_{free}	1206 (118)
R_{work}	0.296 (0.339)
R_{free}	0.345 (0.405)
CC(work)	0.799 (0.738)
CC(free)	0.777 (0.583)
Protein residues	1178
RMS (bonds) (Å)	0.003
RMS (angles) (°)	0.80
Ramachandran favored (%)	94.99
Ramachandran allowed (%)	4.83
Ramachandran outliers (%)	0.18
Rotamer outliers (%)	0.00
Clashscore	13.81
Average B-factor	95.58

Table S2 (related to **Fig. 6**). **Crystallographic data and refinement statistics.** Statistics for the highest-resolution shell are shown in parentheses.

Oligo Name	Sequence - 5' to 3'
MsVHE_F	GGGAATTCGAGGTGCAGCTGCAGGAGTCTGG
CyR_ext1	AGGGAAATARCCCTTGACCAG
CyR_ext2	AGGGAAGTAGCCTTTGACAAG
CyR_int1	GGCCAGTGGATAGACHGATG
CyR_int2	CAGGGACCAAGGGATAGACA
mCk_ext	GCACCTCCAGATGTTAACTG
mCk_int	GATGGTGGGAAGATGGATAC
Vk1_ext	TGATGACCCARACTCCACT
Vk2_ext	GCTTGTGCTCTGGATCCC
Vk3_ext	CTGCTGCTCTGGGTTCC
Vk4_ext	CAGCTTCCTGCTAATCAGTG
Vk5_ext	CTCAGATCCTTGGACTTHTG
Vk6_ext	TGGAGTCACAGACYCAGG
Vk7_ext	TGGAGTTTCAGACCCAGG
Vk8_ext	CTGCTMTGGGTATCTGGT
Vk9_ext	CWTCTTGTTGCTCTGGTTTC
Vk10_ext	GATGTCCTCTGCTCAGTTC
Vk11_ext	CCTGCTGAGTTCCTTGGG
Vk12_ext	CTGCTGCTGTGGCTTACA
Vk13_ext	CCTTCTCAACTTCTGCTCT
Vk14_ext	AGGGCCCYTGCTCAGTTT
Vk15_ext	ATGAGGGTCCTTGCTGAG
Vk16_ext	GAGGTTCCAGGTTCAGGT
Vk17_ext	CCATGACCATGYTCTCACT
Vk18_ext	ATGGAAACTCCAGCTTCATTT
Vk19_ext	ATGAGACCGTCTATTCAGTT
Vk1_int	CCTGTCAGTCTTGGAGATCA
Vk1_2_int	TTTGTCGGTTACCATTGGACAA
Vk2_int	SRGATATTGTGATGACGCAGG
Vk3_int	ATTGTGCTGACCCAATCTCC
Vk4_int	AWTGTKCTCACCCAGTCTCC
Vk5_int	GTCTCCAGCCACCCTGTC
Vk6_int	TGATGACCCAGTCTCMCAAAT
Vk7_int	GCCTGTGCAGACATTGTGAT
Vk8_int	CCTGTGGGGACATTGTGATG
Vk9_int	ACATCCRGATGACYCAGTCT
Vk10_int	CCAGATGTGATATCCAGATG
Vk11_int	GCCAGATGTGATGTYCAAATG
Vk12_int	ATCCAGATGACTCAGTCTCC
Vk13_int	CCTGATATGTGACATCCRVAT
Vk14_int	MAGATGACCCAGTCTCCATC
Vk15_int	TGAGATGTGACATCCAGATGA
Vk16_int	CCAGTGTGATGTCCAGATAAC
Vk17_int	ACAACTGTGACCCAGTCTCC
Vk18_int	ACACAGGCTCCAGCTTCTCT
Vk19_int	GTGCTCAGTGTGACATCCAG

Table S3 (related to **STAR Methods**). **Murine B cell receptor sequencing primers.** Primers originally published in Rohatgi et al., 2008 or Tiller et al., 2009 used for murine B cell receptor sequencing.

B Cell Receptor Sequence	Accession Number
VH_1_A2 variable heavy chain	OM728968
VH_1_A4 variable heavy chain	OM728969
VH_1_A6 variable heavy chain	OM728970
VH_1_A7 variable heavy chain	OM728971
VH_1_A8 variable heavy chain	OM728972
VH_1_A10 variable heavy chain	OM728973
VH_1_A11 variable heavy chain	OM728974
VH_1_B4 variable heavy chain	OM728975
VH_1_B6 variable heavy chain	OM728976
VH_1_B8 variable heavy chain	OM728977
VH_1_B9 variable heavy chain	OM728978
VH_1_B12 variable heavy chain	OM728979
VH_1_C1 variable heavy chain	OM728980
VH_1_C2 variable heavy chain	OM728981
VH_1_C3 variable heavy chain	OM728982
VH_1_C4 variable heavy chain	OM728983
VH_1_C5 variable heavy chain	OM728984
VH_1_C7 variable heavy chain	OM728985
VH_1_C9 variable heavy chain	OM728986
VH_1_C12 variable heavy chain	OM728987
VH_1_D5 variable heavy chain	OM728988
VH_1_D6 variable heavy chain	OM728989
VH_1_D7 variable heavy chain	OM728990
VH_1_D10 variable heavy chain	OM728991
VH_1_D11 variable heavy chain	OM728992
VH_1_D12 variable heavy chain	OM728993
VH_2_A1 variable heavy chain	OM728994
VH_2_A2 variable heavy chain	OM728995
VH_2_A5 variable heavy chain	OM728996
VH_2_A8 variable heavy chain	OM728997
VH_2_B1 variable heavy chain	OM728998
VH_2_B4 variable heavy chain	OM728999
VH_2_B5 variable heavy chain	OM729000
VH_2_B7 variable heavy chain	OM729001
VH_2_B8 variable heavy chain	OM729002
VH_2_C2 variable heavy chain	OM729003
VH_2_C3 variable heavy chain	OM729004
VH_2_C4 variable heavy chain	OM729005
VH_2_C6 variable heavy chain	OM729006
VH_2_C8 variable heavy chain	OM729007
VH_2_C9 variable heavy chain	OM729008
VH_2_C10 variable heavy chain	OM729009
VH_2_C11 variable heavy chain	OM729010
VH_2_D1 variable heavy chain	OM729011
VH_2_D2 variable heavy chain	OM729012
VH_2_D4 variable heavy chain	OM729013
VH_2_D5 variable heavy chain	OM729014
VH_2_D6 variable heavy chain	OM729015

VH_2_D8 variable heavy chain	OM729016
VH_2_D9 variable heavy chain	OM729017
VH_2_D10 variable heavy chain	OM729018
VH_2_D11 variable heavy chain	OM729019
VH_2_E2 variable heavy chain	OM729020
VH_2_E3 variable heavy chain	OM729021
VH_2_E4 variable heavy chain	OM729022
VH_2_E5 variable heavy chain	OM729023
VH_2_E6 variable heavy chain	OM729024
VH_2_E7 variable heavy chain	OM729025
VH_2_E8 variable heavy chain	OM729026
VH_2_E9 variable heavy chain	OM729027
VH_2_E12 variable heavy chain	OM729028
VH_2_F2 variable heavy chain	OM729029
VH_2_F3 variable heavy chain	OM729030
VH_2_F4 variable heavy chain	OM729031
VH_2_F5 variable heavy chain	OM729032
VH_2_F6 variable heavy chain	OM729033
VH_2_F7 variable heavy chain	OM729034
VH_2_F8 variable heavy chain	OM729035
VH_2_F10 variable heavy chain	OM729036
VH_2_F11 variable heavy chain	OM729037
VH_2_F12 variable heavy chain	OM729038
VH_2_G2 variable heavy chain	OM729039
VH_2_G3 variable heavy chain	OM729040
VH_2_G4 variable heavy chain	OM729041
VH_2_G5 variable heavy chain	OM729042
VH_2_G6 variable heavy chain	OM729043
VH_2_G7 variable heavy chain	OM729044
VH_2_G8 variable heavy chain	OM729045
VH_2_G9 variable heavy chain	OM729046
VH_2_G10 variable heavy chain	OM729047
VH_2_G11 variable heavy chain	OM729048
VH_2_H5 variable heavy chain	OM729049
VH_2_H7 variable heavy chain	OM729050
VH_2_H8 variable heavy chain	OM729051
VH_2_H9 variable heavy chain	OM729052
VH_4_A2 variable heavy chain	OM729053
VH_4_A3 variable heavy chain	OM729054
VH_4_A4 variable heavy chain	OM729055
VH_4_A5 variable heavy chain	OM729056
VH_4_A7 variable heavy chain	OM729057
VH_4_A8 variable heavy chain	OM729058
VH_4_A10 variable heavy chain	OM729059
VH_4_B1 variable heavy chain	OM729060
VH_4_B2 variable heavy chain	OM729061
VH_4_B3 variable heavy chain	OM729062
VH_4_B4 variable heavy chain	OM729063
VH_4_B5 variable heavy chain	OM729064

VH_4_B6 variable heavy chain	OM729065
VH_4_B8 variable heavy chain	OM729066
VH_4_C2 variable heavy chain	OM729067
VH_4_C3 variable heavy chain	OM729068
VH_4_C6 variable heavy chain	OM729069
VH_4_C8 variable heavy chain	OM729070
VH_4_C9 variable heavy chain	OM729071
VH_4_C10 variable heavy chain	OM729072
VH_4_C11 variable heavy chain	OM729073
VH_4_C12 variable heavy chain	OM729074
VH_4_D2 variable heavy chain	OM729075
VH_4_D3 variable heavy chain	OM729076
VH_4_D4 variable heavy chain	OM729077
VH_4_D5 variable heavy chain	OM729078
VH_4_D6 variable heavy chain	OM729079
VH_4_D7 variable heavy chain	OM729080
VH_4_D9 variable heavy chain	OM729081
VH_4_D10 variable heavy chain	OM729082
VH_5_A2 variable heavy chain	OM729083
VH_5_A3 variable heavy chain	OM729084
VH_5_A6 variable heavy chain	OM729085
VH_5_A10 variable heavy chain	OM729086
VH_5_A12 variable heavy chain	OM729087
VH_5_B1 variable heavy chain	OM729088
VH_5_B3 variable heavy chain	OM729089
VH_5_B4 variable heavy chain	OM729090
VH_5_B5 variable heavy chain	OM729091
VH_5_B8 variable heavy chain	OM729092
VH_5_B9 variable heavy chain	OM729093
VH_5_B12 variable heavy chain	OM729094
VH_5_C1 variable heavy chain	OM729095
VH_5_C2 variable heavy chain	OM729096
VH_5_C3 variable heavy chain	OM729097
VH_5_C4 variable heavy chain	OM729098
VH_5_C6 variable heavy chain	OM729099
VH_5_C8 variable heavy chain	OM729100
VH_5_C9 variable heavy chain	OM729101
VH_5_C11 variable heavy chain	OM729102
VH_5_D1 variable heavy chain	OM729103
VH_5_D3 variable heavy chain	OM729104
VH_5_D4 variable heavy chain	OM729105
VH_5_D6 variable heavy chain	OM729106
VH_5_D7 variable heavy chain	OM729107
VH_5_D8 variable heavy chain	OM729108
VH_5_D9 variable heavy chain	OM729109
VH_5_D11 variable heavy chain	OM729110
VH_5_D12 variable heavy chain	OM729111
VH_5_E1 variable heavy chain	OM729112
VH_5_E3 variable heavy chain	OM729113

VH_5_E5 variable heavy chain	OM729114
VH_5_E6 variable heavy chain	OM729115
VH_5_E7 variable heavy chain	OM729116
VH_5_E9 variable heavy chain	OM729117
VH_5_E10 variable heavy chain	OM729118
VH_5_E11 variable heavy chain	OM729119
VH_5_E12 variable heavy chain	OM729120
VH_5_F1 variable heavy chain	OM729121
VH_5_F2 variable heavy chain	OM729122
VH_5_F3 variable heavy chain	OM729123
VH_5_F5 variable heavy chain	OM729124
VH_5_F6 variable heavy chain	OM729125
VH_5_F8 variable heavy chain	OM729126
VH_5_F10 variable heavy chain	OM729127
VH_5_F12 variable heavy chain	OM729128
VH_5_G1 variable heavy chain	OM729129
VH_5_G2 variable heavy chain	OM729130
VH_5_G3 variable heavy chain	OM729131
VH_5_G4 variable heavy chain	OM729132
VH_5_G5 variable heavy chain	OM729133
VH_5_G6 variable heavy chain	OM729134
VH_5_G7 variable heavy chain	OM729135
VH_5_G9 variable heavy chain	OM729136
VH_5_G10 variable heavy chain	OM729137
VH_5_G12 variable heavy chain	OM729138
VH_5_H1 variable heavy chain	OM729139
VH_5_H4 variable heavy chain	OM729140
VH_5_H6 variable heavy chain	OM729141
VH_5_H8 variable heavy chain	OM729142
VH_5_H11 variable heavy chain	OM729143
VL_1_A2 variable light chain	OM729144
VL_1_A4 variable light chain	OM729145
VL_1_A6 variable light chain	OM729146
VL_1_A7 variable light chain	OM729147
VL_1_A8 variable light chain	OM729148
VL_1_A10 variable light chain	OM729149
VL_1_A11 variable light chain	OM729150
VL_1_B4 variable light chain	OM729151
VL_1_B6 variable light chain	OM729152
VL_1_B8 variable light chain	OM729153
VL_1_B9 variable light chain	OM729154
VL_1_B12 variable light chain	OM729155
VL_1_C1 variable light chain	OM729156
VL_1_C2 variable light chain	OM729157
VL_1_C3 variable light chain	OM729158
VL_1_C4 variable light chain	OM729159
VL_1_C5 variable light chain	OM729160
VL_1_C7 variable light chain	OM729161
VL_1_C9 variable light chain	OM729162

VL_1_C12 variable light chain	OM729163
VL_1_D5 variable light chain	OM729164
VL_1_D6 variable light chain	OM729165
VL_1_D7 variable light chain	OM729166
VL_1_D10 variable light chain	OM729167
VL_1_D11 variable light chain	OM729168
VL_1_D12 variable light chain	OM729169
VL_2_A1 variable light chain	OM729170
VL_2_A2 variable light chain	OM729171
VL_2_A5 variable light chain	OM729172
VL_2_A8 variable light chain	OM729173
VL_2_B1 variable light chain	OM729174
VL_2_B4 variable light chain	OM729175
VL_2_B5 variable light chain	OM729176
VL_2_B7 variable light chain	OM729177
VL_2_B8 variable light chain	OM729178
VL_2_C2 variable light chain	OM729179
VL_2_C3 variable light chain	OM729180
VL_2_C4 variable light chain	OM729181
VL_2_C6 variable light chain	OM729182
VL_2_C8 variable light chain	OM729183
VL_2_C9 variable light chain	OM729184
VL_2_C10 variable light chain	OM729185
VL_2_C11 variable light chain	OM729186
VL_2_D1 variable light chain	OM729187
VL_2_D2 variable light chain	OM729188
VL_2_D4 variable light chain	OM729189
VL_2_D5 variable light chain	OM729190
VL_2_D6 variable light chain	OM729191
VL_2_D8 variable light chain	OM729192
VL_2_D9 variable light chain	OM729193
VL_2_D10 variable light chain	OM729194
VL_2_D11 variable light chain	OM729195
VL_2_E2 variable light chain	OM729196
VL_2_E3 variable light chain	OM729197
VL_2_E4 variable light chain	OM729198
VL_2_E5 variable light chain	OM729199
VL_2_E6 variable light chain	OM729200
VL_2_E7 variable light chain	OM729201
VL_2_E8 variable light chain	OM729202
VL_2_E9 variable light chain	OM729203
VL_2_E12 variable light chain	OM729204
VL_2_F2 variable light chain	OM729205
VL_2_F3 variable light chain	OM729206
VL_2_F4 variable light chain	OM729207
VL_2_F5 variable light chain	OM729208
VL_2_F6 variable light chain	OM729209
VL_2_F7 variable light chain	OM729210
VL_2_F8 variable light chain	OM729211

VL_2_F10 variable light chain	OM729212
VL_2_F11 variable light chain	OM729213
VL_2_F12 variable light chain	OM729214
VL_2_G2 variable light chain	OM729215
VL_2_G3 variable light chain	OM729216
VL_2_G4 variable light chain	OM729217
VL_2_G5 variable light chain	OM729218
VL_2_G6 variable light chain	OM729219
VL_2_G7 variable light chain	OM729220
VL_2_G8 variable light chain	OM729221
VL_2_G9 variable light chain	OM729222
VL_2_G10 variable light chain	OM729223
VL_2_G11 variable light chain	OM729224
VL_2_H5 variable light chain	OM729225
VL_2_H7 variable light chain	OM729226
VL_2_H8 variable light chain	OM729227
VL_2_H9 variable light chain	OM729228
VL_4_A2 variable light chain	OM729229
VL_4_A3 variable light chain	OM729230
VL_4_A4 variable light chain	OM729231
VL_4_A5 variable light chain	OM729232
VL_4_A7 variable light chain	OM729233
VL_4_A8 variable light chain	OM729234
VL_4_A10 variable light chain	OM729235
VL_4_B1 variable light chain	OM729236
VL_4_B2 variable light chain	OM729237
VL_4_B3 variable light chain	OM729238
VL_4_B4 variable light chain	OM729239
VL_4_B5 variable light chain	OM729240
VL_4_B6 variable light chain	OM729241
VL_4_B8 variable light chain	OM729242
VL_4_C2 variable light chain	OM729243
VL_4_C3 variable light chain	OM729244
VL_4_C6 variable light chain	OM729245
VL_4_C8 variable light chain	OM729246
VL_4_C9 variable light chain	OM729247
VL_4_C10 variable light chain	OM729248
VL_4_C11 variable light chain	OM729249
VL_4_C12 variable light chain	OM729250
VL_4_D2 variable light chain	OM729251
VL_4_D3 variable light chain	OM729252
VL_4_D4 variable light chain	OM729253
VL_4_D5 variable light chain	OM729254
VL_4_D6 variable light chain	OM729255
VL_4_D7 variable light chain	OM729256
VL_4_D9 variable light chain	OM729257
VL_4_D10 variable light chain	OM729258
VL_5_A2 variable light chain	OM729259
VL_5_A3 variable light chain	OM729260

VL_5_A6 variable light chain	OM729261
VL_5_A10 variable light chain	OM729262
VL_5_A12 variable light chain	OM729263
VL_5_B1 variable light chain	OM729264
VL_5_B3 variable light chain	OM729265
VL_5_B4 variable light chain	OM729266
VL_5_B5 variable light chain	OM729267
VL_5_B8 variable light chain	OM729268
VL_5_B9 variable light chain	OM729269
VL_5_B12 variable light chain	OM729270
VL_5_C1 variable light chain	OM729271
VL_5_C2 variable light chain	OM729272
VL_5_C3 variable light chain	OM729273
VL_5_C4 variable light chain	OM729274
VL_5_C6 variable light chain	OM729275
VL_5_C8 variable light chain	OM729276
VL_5_C9 variable light chain	OM729277
VL_5_C11 variable light chain	OM729278
VL_5_D1 variable light chain	OM729279
VL_5_D3 variable light chain	OM729280
VL_5_D4 variable light chain	OM729281
VL_5_D6 variable light chain	OM729282
VL_5_D7 variable light chain	OM729283
VL_5_D8 variable light chain	OM729284
VL_5_D9 variable light chain	OM729285
VL_5_D11 variable light chain	OM729286
VL_5_D12 variable light chain	OM729287
VL_5_E1 variable light chain	OM729288
VL_5_E3 variable light chain	OM729289
VL_5_E5 variable light chain	OM729290
VL_5_E6 variable light chain	OM729291
VL_5_E7 variable light chain	OM729292
VL_5_E9 variable light chain	OM729293
VL_5_E10 variable light chain	OM729294
VL_5_E11 variable light chain	OM729295
VL_5_E12 variable light chain	OM729296
VL_5_F1 variable light chain	OM729297
VL_5_F2 variable light chain	OM729298
VL_5_F3 variable light chain	OM729299
VL_5_F5 variable light chain	OM729300
VL_5_F6 variable light chain	OM729301
VL_5_F8 variable light chain	OM729302
VL_5_F10 variable light chain	OM729303
VL_5_F12 variable light chain	OM729304
VL_5_G1 variable light chain	OM729305
VL_5_G2 variable light chain	OM729306
VL_5_G3 variable light chain	OM729307
VL_5_G4 variable light chain	OM729308
VL_5_G5 variable light chain	OM729309

VL_5_G6 variable light chain	OM729310
VL_5_G7 variable light chain	OM729311
VL_5_G9 variable light chain	OM729312
VL_5_G10 variable light chain	OM729313
VL_5_G12 variable light chain	OM729314
VL_5_H1 variable light chain	OM729315
VL_5_H4 variable light chain	OM729316
VL_5_H6 variable light chain	OM729317
VL_5_H8 variable light chain	OM729318
VL_5_H11 variable light chain	OM729319

Table S4 (related to **STAR Methods**). **Murine B cell receptor sequence accession numbers.**
Genbank accession numbers for B cell receptor sequences.